Real-Time Hybrid Simulation of Complex Structures using Multi-Actuator Control

B.M. Phillips & B.F. Spencer, Jr.
University of Illinois

SUMMARY:
Hybrid simulation combines numerical simulation and experimental testing in a loop of action and reaction to capture the dynamic behavior of a structure. When the rate-dependent behavior of the experimental component is significant, the hybrid simulation must be conducted in real-time (i.e., real-time hybrid simulation or RTHS). In RTHS, the actuator dynamics are directly introduced into the RTHS loop. Also, the phenomenon of control-structure interaction leads to a coupling of the behavior of the actuators and specimen. Traditional actuator control approaches compensate for an apparent time delay or time lag rather than address the actuator dynamics directly. Moreover, most actuator control approaches focus on single-actuator systems. The control approach proposed herein directly addresses actuator dynamics through model-based feedforward-feedback control. The modeling captures the dynamic coupling between the actuators, ensuring accurate control for multi-actuator systems. The proposed approach is illustrated for the RTHS of a three-story building with multiple actuators.

Keywords: Real-time hybrid simulation, Multi-actuator systems, Actuator control, Actuator coupling

1. INTRODUCTION

Real-time hybrid simulation (RTHS) requires accurate tracking of desired displacements using servo-hydraulic actuators. Close examination of the servo-hydraulic system response shows that experimental equipment introduces both time delays and frequency-dependent time lags into the RTHS loop. Time delays and lags are an intrinsic part of experimental testing, and mitigation of their effects is an essential part of RTHS. In addition, coupling of the dynamics between the actuator and specimen was observed and explained by Dyke *et al.* (1995) and identified as the phenomenon of control-structure interaction (CSI). Prior to this study, researchers have neglected actuator dynamics and CSI in experimental testing. This oversight was acceptable for slow-speed tests including conventional hybrid simulation, but unacceptable for the emerging framework of RTHS.

CSI has been well studied for single-actuator systems, and RTHS actuator control approaches considering specimen dependency through CSI have been proposed (Carrion and Spencer, 2007; Phillips and Spencer, 2011). However, as RTHS is being used for more complex tests, control of multiple actuators will be required. For multi-actuator systems, CSI leads to a complex actuator control challenge. Because the dynamics of a single actuator are coupled to a specimen, when multiple actuators are connected to the same specimen, the dynamics of all of the actuators become coupled to each other through the specimen.

A model-based approach to multi-actuator control is proposed in this paper. Both the dynamic behavior of the actuators and the dynamic coupling between actuators are considered, assuring accurate control in the presence of CSI. The efficacy of the proposed approach is illustrated through numerical simulation of a three-story steel building with multiple actuators used to control the structure in RTHS.

1.1. Problem Formulation

In hybrid simulation, the equations of motion governing the dynamic response of a structure can be separated into numerical and experimental components as indicated by superscripts "N" and "E", respectively:

$$\mathbf{M}^{\mathrm{N}}\ddot{\mathbf{x}}+\mathbf{C}^{\mathrm{N}}\dot{\mathbf{x}}+\mathbf{K}^{\mathrm{N}}\mathbf{x}+\mathbf{R}^{\mathrm{E}}\left(\mathbf{x},\dot{\mathbf{x}},\ddot{\mathbf{x}}\right)=-\left(\mathbf{M}^{\mathrm{N}}+\mathbf{M}^{\mathrm{E}}\right)\mathbf{\Gamma}\ddot{x}_{\mathrm{g}} \tag{1.1}$$

where $\mathbf{M}$ is the mass matrix, $\mathbf{C}$ is the damping matrix, $\mathbf{K}$ is stiffness matrix, $\mathbf{\Gamma}$ is the mass influence matrix, $\ddot{x}_{\mathrm{g}}$ is the ground acceleration, $\mathbf{x}$ is the displacement vector relative to the ground, and dots represent differentiation with respect to time. The restoring force of the experimental component is lumped into the vector $\mathbf{R}^{\mathrm{E}}$, which contains static, damping, and inertial forces. A linear system is presented for clarity, although the formulation can be adapted to include nonlinear systems.

The loop of action and reaction between numerical and experimental components during RTHS is illustrated in Fig. 1.1. From numerical integration of Eqn. 1.1, the structure is excited and displacements $\mathbf{x}$ are calculated. To achieve compatibility between numerical and experimental components, the subset of $\mathbf{x}$ corresponding to the interface DOFs $\mathbf{x}^{\mathrm{I}}$ are commanded to the experimental component using servo-hydraulic actuators. Inner-loop feedback control (through the servo-controller) provides nominal tracking of the command vector $\mathbf{u}$ as measured by $\mathbf{x}^{\mathrm{E}}$, the vector of interface degrees-of-freedom (DOFs) physically realized by the experimental component. Outer-loop actuator control is typically added to determine $\mathbf{u}$ such that $\mathbf{x}^{\mathrm{E}}$ tracks $\mathbf{x}^{\mathrm{I}}$ very accurately and in real-time. The restoring forces of the specimen, as measured by the actuator load cells or external load cells, are returned to the numerical integration scheme as $\mathbf{R}^{\mathrm{E}}$. The natural velocity feedback captures the specimen dependency of the servo-hydraulic system through CSI (Dyke *et al.*, 1995).

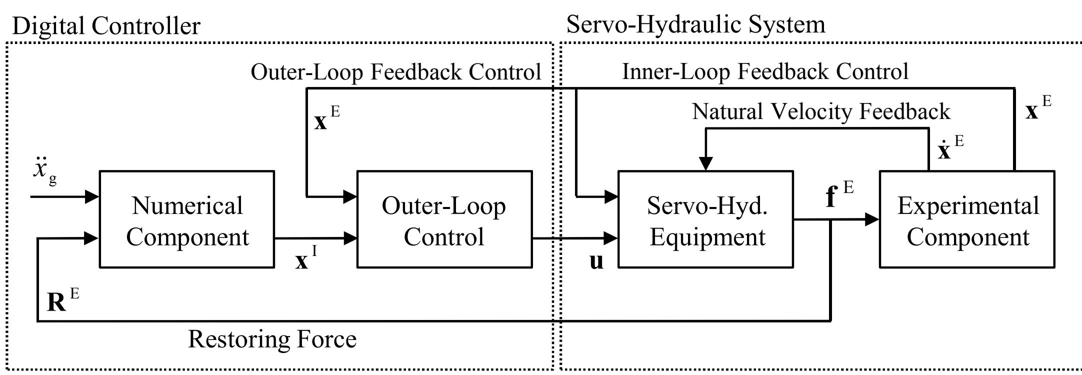

Figure 1.1. Multiple feedback loops in RTHS

In model-based control, the outer-loop controller is created to cancel out the dynamics of the servo-hydraulic system. Consider the input-output transfer function model $\mathbf{G}_{xu}\left(s\right)$ of the linearized servo-hydraulic system, including the actuator, servo-valve, servo-controller, and specimen (experimental component) as represented in Fig. 1.2 and based on Dyke *et al.* (1995).

The dynamics of the servo-controller and servo-valve, actuator, and specimen have been condensed into transfer functions $\mathbf{G}_{\mathrm{s}}\left(s\right)$, $\mathbf{G}_{\mathrm{a}}\left(s\right)$, and $\mathbf{G}_{xf}\left(s\right)$, respectively. The matrix $\mathbf{A}$ represents the effective cross-sectional area of the actuator piston. The input-output transfer function, applicable to both single-input single-output (SISO) and multi-input multi-output (MIMO) systems, is written as:

$$\mathbf{G}_{xu}\left(s\right)=\frac{\mathbf{X}^{\mathrm{E}}\left(s\right)}{\mathbf{U}\left(s\right)}=\frac{\mathbf{G}_{\mathrm{s}}\left(s\right)\mathbf{G}_{\mathrm{a}}\left(s\right)\mathbf{G}_{xf}\left(s\right)}{\mathbf{I}+\left(\mathbf{G}_{\mathrm{s}}\left(s\right)+\mathbf{A}s\right)\mathbf{G}_{\mathrm{a}}\left(s\right)\mathbf{G}_{xf}\left(s\right)} \tag{1.2}$$

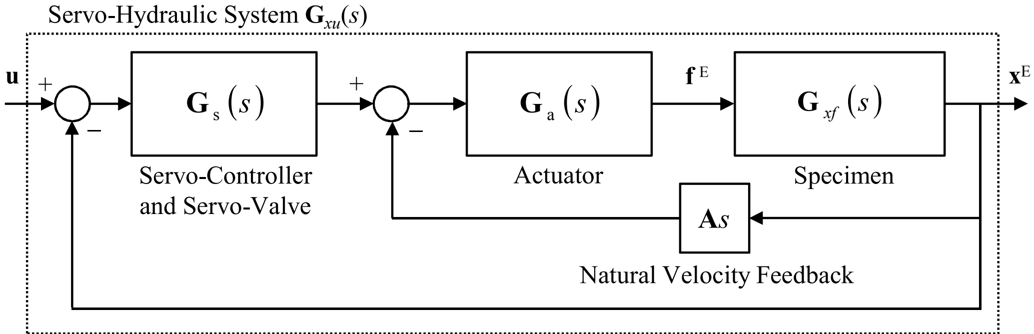

Figure 1.2. Servo-hydraulic system with CSI

1.2. Illustration of Actuator Coupling

When multiple actuators are connected to the same specimen, the dynamics of the actuators become coupled through the specimen (i.e., when an actuator applies a force to the structure, the other actuators will also experience this force). This section demonstrates such coupling using the three-degree-of-freedom (3DOF) linear building structure shown in Fig. 1.3.

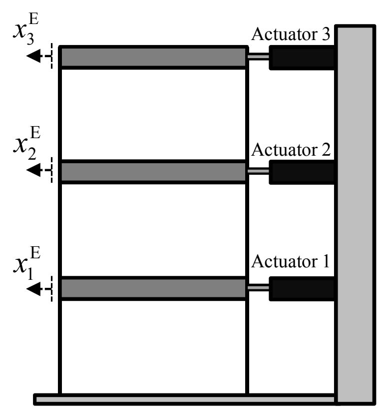

Figure 1.3. Example 3DOF linear structure

The structure employs three servo-hydraulic systems, each comprised of a servo-valve, a servo-controller, and an actuator and can be represented in Fig. 1.2 by the following diagonal matrices:

$$\mathbf{G}_s(s) = \mathrm{diag}(k_{s1}, k_{s2}, k_{s3}) \qquad \mathbf{G}_a(s) = \mathrm{diag}\left(\frac{k_{a1}}{(s - p_{a1})}, \frac{k_{a2}}{(s - p_{a2})}, \frac{k_{a3}}{(s - p_{a3})}\right) \qquad \mathbf{A} = \mathrm{diag}(A_1, A_2, A_3) \tag{1.3}$$

The servo-controller and servo-valve dynamics are chosen as a constant gain, the actuator dynamics are chosen as a first-order model, and the effective cross-sectional area is a constant. Such a selection is consistent with the models presented in Dyke *et al.* (1995) for single-actuator systems. The commanded displacements, measured forces, and measured displacements of Fig 1.2 are written as $\mathbf{u} = \{u_1 \quad u_2 \quad u_3\}^T$, $\mathbf{f}^E = \{f_1^E \quad f_2^E \quad f_3^E\}^T$, and $\mathbf{x}^E = \{x_1^E \quad x_2^E \quad x_3^E\}^T$, respectively.

For generality, the mass, damping, and stiffness matrices of the structure are assumed fully populated. The transfer function relating the input force from the actuators to the output displacement is given by:

$$\mathbf{G}_{xf}(s) = \frac{\mathbf{X}^E(s)}{\mathbf{F}(s)} = \left[\mathbf{M}^E s^2 + \mathbf{C}^E s + \mathbf{K}^E\right]^{-1} = \begin{bmatrix} m_{11}^E s^2 + c_{11}^E s + k_{11}^E & m_{12}^E s^2 + c_{12}^E s + k_{12}^E & m_{13}^E s^2 + c_{13}^E s + k_{13}^E \\ m_{21}^E s^2 + c_{21}^E s + k_{21}^E & m_{22}^E s^2 + c_{22}^E s + k_{22}^E & m_{23}^E s^2 + c_{23}^E s + k_{23}^E \\ m_{31}^E s^2 + c_{31}^E s + k_{31}^E & m_{32}^E s^2 + c_{32}^E s + k_{32}^E & m_{33}^E s^2 + c_{33}^E s + k_{33}^E \end{bmatrix}^{-1} \tag{1.4}$$

where m, c, and k represent entries in the mass, damping, and stiffness matrices, respectively, with their position indicated by the subscripts. The off-diagonal terms in Eqn. 1.4 are the source of the interaction between the three servo-hydraulic systems. Substituting Eqns. 1.3 and 1.4 into 1.2, the MIMO servo-hydraulic system transfer function model is obtained:

$$\mathbf{G}_{xu}(s)=\frac{\mathbf{X}^{\mathrm{E}}(s)}{\mathbf{U}(s)}=\frac{\begin{bmatrix}\prod_{i=1}^{6}(s-z_{11,i}) & \prod_{i=1}^{6}(s-z_{12,i}) & \prod_{i=1}^{6}(s-z_{13,i})\\ \prod_{i=1}^{6}(s-z_{21,i}) & \prod_{i=1}^{6}(s-z_{22,i}) & \prod_{i=1}^{6}(s-z_{23,i})\\ \prod_{i=1}^{6}(s-z_{31,i}) & \prod_{i=1}^{6}(s-z_{32,i}) & \prod_{i=1}^{6}(s-z_{33,i})\end{bmatrix}}{\prod_{i=1}^{9}(s-p_i)} \tag{1.5}$$

where z and p represent the model zeros and poles, respectively. The poles and zeros can be obtained in closed-form, although they are too complicated for concise presentation. In Eqn. 1.5, the off-diagonal terms describe the interaction between the three servo-hydraulic systems.

2. MODEL-BASED CONTROL OF MIMO SYSTEM

The model-based control approach proposed herein is based on a linearized model of the servo-hydraulic system, as in Eqn. 1.2, which is represented in state space form to facilitate modern control theory design (Phillips and Spencer, 2011):

$$\dot{\mathbf{z}}=\mathbf{Az}+\mathbf{Bu} \tag{2.1}$$

$$\mathbf{x}^{\mathrm{E}}=\mathbf{Cz} \tag{2.2}$$

where $\mathbf{z}$ is the state vector and **A**, **B**, and **C** are the system, input, and output matrices, respectively. The tracking error between the desired and measured displacement (or $\mathbf{x}^{\mathrm{I}}$ and $\mathbf{x}^{\mathrm{E}}$, respectively) is defined as $\mathbf{e}=\mathbf{x}^{\mathrm{I}}-\mathbf{x}^{\mathrm{E}}$. The command $\mathbf{u}$ to the actuator should be chosen such that the tracking error is minimized. If perfect tracking is achieved, an ideal state $\overline{\mathbf{z}}$ and an ideal input $\overline{\mathbf{u}}$ leading to an output $\overline{\mathbf{x}}^{\mathrm{E}}$ must exist such that $\overline{\mathbf{x}}^{\mathrm{E}}=\mathbf{x}^{\mathrm{I}}$. The ideal system is described as:

$$\dot{\overline{\mathbf{z}}}=\mathbf{A}\overline{\mathbf{z}}+\mathbf{B}\overline{\mathbf{u}} \tag{2.3}$$

$$\overline{\mathbf{x}}^{\mathrm{E}}=\mathbf{C}\overline{\mathbf{z}}=\mathbf{x}^{\mathrm{I}} \tag{2.4}$$

Deviations of the state, control, and output from this ideal system with respect to the original system are defined as $\tilde{\mathbf{z}}=\mathbf{z}-\overline{\mathbf{z}}$, $\tilde{\mathbf{u}}=\mathbf{u}-\overline{\mathbf{u}}$, and $\tilde{\mathbf{x}}^{\mathrm{E}}=\mathbf{x}^{\mathrm{E}}-\overline{\mathbf{x}}^{\mathrm{E}}$. The dynamics of the deviation system are then:

$$\dot{\tilde{\mathbf{z}}}=\mathbf{A}\tilde{\mathbf{z}}+\mathbf{B}\tilde{\mathbf{u}} \tag{2.5}$$

$$\tilde{\mathbf{x}}^{\mathrm{E}}=\mathbf{C}\tilde{\mathbf{z}}=-\mathbf{e} \tag{2.6}$$

The tracking problem has now been redefined as a regulator problem about a setpoint (Lewis and Syrmos, 1995). The control law $\tilde{\mathbf{u}}=\mathbf{u}-\overline{\mathbf{u}}$ can be rewritten in terms of the original system command $\mathbf{u}$, which consists of a feedforward component $\overline{\mathbf{u}}=\mathbf{u}_{\mathrm{FF}}$ determined from the ideal system and a feedback component $\tilde{\mathbf{u}}=\mathbf{u}_{\mathrm{FB}}$ determined from the deviation system.

The model-based controller, incorporating both feedforward and feedback links, is represented schematically in Fig. 2.1. The servo-hydraulic system of Fig. 1.2 has been condensed to show the details of the model-based controller, which acts as an outer-loop controller around the system.

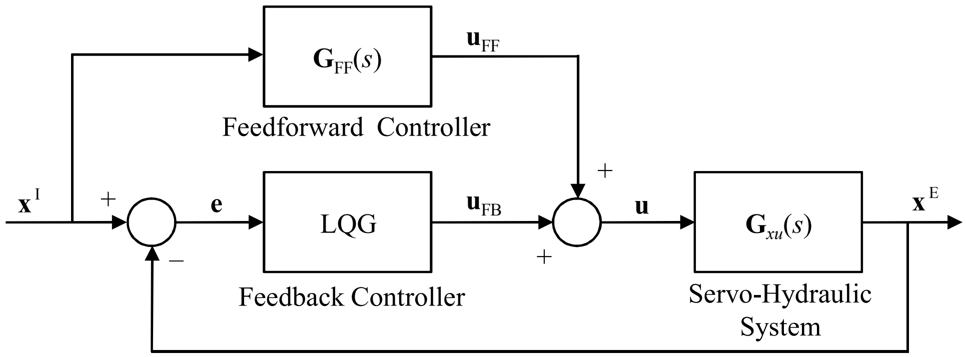

Figure 2.1. Model-based actuator control with feedforward and feedback links

2.1. Feedforward Control

The feedforward controller is designed to cancel the modeled dynamics of the servo-hydraulic system. The inverse of the servo-hydraulic system model will serve as the feedforward controller:

$$\mathbf{G}_{\mathrm{FF}}(s) = \mathbf{G}_{xu}(s)^{-1} = \frac{\mathbf{U}_{\mathrm{FF}}(s)}{\mathbf{X}^{\mathrm{I}}(s)} = \mathbf{I} + \mathbf{G}_{xu}(s)^{-1}\,\mathbf{G}_{\mathrm{a}}(s)^{-1}\,\mathbf{G}_{\mathrm{s}}(s)^{-1} + \mathbf{A}s\mathbf{G}_{\mathrm{s}}(s)^{-1} \tag{2.7}$$

Substituting Eqns. 1.3 and 1.4 into 2.7 yields:

$$\mathbf{G}_{\mathbf{FF}}(s) = \begin{bmatrix} \left(m_{11}^{\mathrm{E}}s^2 + c_{11}^{\mathrm{E}}s + k_{11}^{\mathrm{E}}\right)\dfrac{(s-p_{\mathrm{a1}})}{k_{\mathrm{a1}}k_{\mathrm{s1}}} + \dfrac{sA_1}{k_{\mathrm{s1}}} + 1 & \left(m_{12}^{\mathrm{E}}s^2 + c_{12}^{\mathrm{E}}s + k_{12}^{\mathrm{E}}\right)\dfrac{(s-p_{\mathrm{a2}})}{k_{\mathrm{a2}}k_{\mathrm{s2}}} & \left(m_{13}^{\mathrm{E}}s^2 + c_{13}^{\mathrm{E}}s + k_{13}^{\mathrm{E}}\right)\dfrac{(s-p_{\mathrm{a3}})}{k_{\mathrm{a3}}k_{\mathrm{s3}}} \\ \left(m_{21}^{\mathrm{E}}s^2 + c_{21}^{\mathrm{E}}s + k_{21}^{\mathrm{E}}\right)\dfrac{(s-p_{\mathrm{a1}})}{k_{\mathrm{a1}}k_{\mathrm{s1}}} & \left(m_{22}^{\mathrm{E}}s^2 + c_{22}^{\mathrm{E}}s + k_{22}^{\mathrm{E}}\right)\dfrac{(s-p_{\mathrm{a2}})}{k_{\mathrm{a2}}k_{\mathrm{s2}}} + \dfrac{sA_2}{k_{\mathrm{s2}}} + 1 & \left(m_{32}^{\mathrm{E}}s^2 + c_{32}^{\mathrm{E}}s + k_{32}^{\mathrm{E}}\right)\dfrac{(s-p_{\mathrm{a3}})}{k_{\mathrm{a3}}k_{\mathrm{s3}}} \\ \left(m_{31}^{\mathrm{E}}s^2 + c_{31}^{\mathrm{E}}s + k_{31}^{\mathrm{E}}\right)\dfrac{(s-p_{\mathrm{a1}})}{k_{\mathrm{a1}}k_{\mathrm{s1}}} & \left(m_{32}^{\mathrm{E}}s^2 + c_{32}^{\mathrm{E}}s + k_{32}^{\mathrm{E}}\right)\dfrac{(s-p_{\mathrm{a2}})}{k_{\mathrm{a2}}k_{\mathrm{s2}}} & \left(m_{33}^{\mathrm{E}}s^2 + c_{33}^{\mathrm{E}}s + k_{33}^{\mathrm{E}}\right)\dfrac{(s-p_{\mathrm{a3}})}{k_{\mathrm{a3}}k_{\mathrm{s3}}} + \dfrac{sA_3}{k_{\mathrm{s3}}} + 1 \end{bmatrix} \tag{2.8}$$

Equation 2.8 is relatively simple compared to Eqn. 1.5. For each input-output pair, there are two zeros that appear as a result of the second-order specimen dynamics. If the mass, damping, or stiffness matrices are not fully populated, as in a lumped mass system or a shear building, then Eqn. 2.8 could be further simplified. Thus, an understanding of the behavior of the physical specimen can aid in determining the number of zeros (and poles) to use in the feedforward controller. A third zero in each input-output pair arises from the first-order actuator model.

The feedforward controller of Eqn 2.8 is improper. The proposed approach for accommodating the improper transfer function is to make use of higher order derivatives which are available from numerical integration during RTHS. Methods for accurately estimating the higher-order derivatives during RTHS are discussed in Phillips and Spencer (2011).

2.2. Feedback Control

In the presence of changing specimen conditions, modeling errors, nonlinearities, and disturbances, feedback control can be applied to reduce further the tracking error by bringing the deviation states of Eqn. 2.5 to zero. Evoking the separation principal, an LQG controller can be designed from independent LQR (optimal state feedback control) and Kalman filter (optimal observer) designs. To improve the LQG controller's performance and robustness in the frequency range of interest, a shaping filter can be added to the process noise as in Phillips and Spencer (2011).

Model-based feedback control is derived from a state space representation of the transfer function given in Eqn. 1.2. By examining the dynamics of Fig. 1.2, the following state space realization can be create directly:

$$\begin{Bmatrix} \dot{x}_1^{\mathrm{E}} \\ \dot{x}_2^{\mathrm{E}} \\ \dot{x}_3^{\mathrm{E}} \\ \ddot{x}_1^{\mathrm{E}} \\ \ddot{x}_2^{\mathrm{E}} \\ \ddot{x}_3^{\mathrm{E}} \\ \dot{f}_1^{\mathrm{E}} \\ \dot{f}_2^{\mathrm{E}} \\ \dot{f}_3^{\mathrm{E}} \end{Bmatrix} = \begin{bmatrix} 0_{3\times3} & \mathrm{I}_{3\times3} & 0_{3\times3} \\ -\left(M^{\mathrm{E}}\right)^{-1} K^{\mathrm{E}} & -\left(M^{\mathrm{E}}\right)^{-1} C^{\mathrm{E}} & \left(M^{\mathrm{E}}\right)^{-1} \\ \begin{pmatrix} -k_{a1}k_{s1} & 0 & 0 \\ 0 & -k_{a2}k_{s2} & 0 \\ 0 & 0 & -k_{a3}k_{s3} \end{pmatrix} & \begin{pmatrix} -k_{a1}A_1 & 0 & 0 \\ 0 & -k_{a2}A_2 & 0 \\ 0 & 0 & -k_{a3}A_3 \end{pmatrix} & \begin{pmatrix} p_{a1} & 0 & 0 \\ 0 & p_{a2} & 0 \\ 0 & 0 & p_{a3} \end{pmatrix} \end{bmatrix} \begin{Bmatrix} x_1^{\mathrm{E}} \\ x_2^{\mathrm{E}} \\ x_3^{\mathrm{E}} \\ \dot{x}_1^{\mathrm{E}} \\ \dot{x}_2^{\mathrm{E}} \\ \dot{x}_3^{\mathrm{E}} \\ f_1^{\mathrm{E}} \\ f_2^{\mathrm{E}} \\ f_3^{\mathrm{E}} \end{Bmatrix} + \begin{bmatrix} 0_{3\times3} \\ 0_{3\times3} \\ \begin{pmatrix} k_{a1}k_{s1} & 0 & 0 \\ 0 & k_{a2}k_{s2} & 0 \\ 0 & 0 & k_{a3}k_{s3} \end{pmatrix} \end{bmatrix} \begin{Bmatrix} u_1 \\ u_2 \\ u_3 \end{Bmatrix} \tag{2.9}$$

As expected, the state space model contains nine poles. In a practical situation where the specimen dynamics must be obtained from system identification, identifying the inverse first and then calculating the servo-hydraulic system transfer function model from this inverse may be preferred. Such an approach is discussed and applied for the following example.

The preceding model-based multi-actuator control scheme was presented for a three-actuator system. The same approach can be applied to an arbitrary number of actuators. Likewise, the approach can be easily adapted to higher-order servo-hydraulic system models as needed.

3. RTHS OF A NONLINEAR MDOF STRUCTURE

To demonstrate the performance of the proposed model-based multi-actuator control strategy, a semi-actively controlled multi-degree-of-freedom (MDOF) building is considered. For simplicity, all DOF are selected as interface DOF (having both numerical and experimental components). The experimental component is selected as the small-scale three-story building model from multiple studies on active and semi-active control (Dyke *et al.*, 1995; Dyke *et al.*, 1996). The natural frequencies are 5.46, 15.8, and 23.6 Hz, with damping ratios of 0.31, 0.62, and 0.63%. A numerical component is added with a mass matrix equal to 9 times the mass matrix of the experimental component, bringing the natural frequencies of the total structure (combining numerical and experimental components) to 1.73, 5.00, and 7.48 Hz. Rayleigh damping is added to the total structure to create damping ratios of 1.00, 1.00, and 1.57%. The additional damping required to achieve these damping ratios is added numerically. Finally, a small-scale MR damper is added between the ground and first story of the structure. This MR damper is considered part of the experimental component and modeled using the phenomenological model and parameters proposed by Spencer *et al.* (1997). The MR damper has a maximum force of approximately 1.5 kN, which is about 5% of the seismic mass of the total structure. The numerical and experimental components are illustrated in Fig. 3.1. Servo-hydraulic actuators are connected to each of the three floors of the experimental structure to enforce compatibility with the numerical component and provide restoring force feedback from the load cells. The servo-hydraulic system parameters for all three actuators are based on the small-scale actuator model of Dyke *et al.* (1995).

The experimental component is assumed to be equipped with sensors measuring the actuator displacements, the restoring forces, the absolute story accelerations, the MR damper displacement, and the MR damper restoring force with simulated measurement noise. The absolute story accelerations, the MR damper displacement, and the MR damper force are available to a semi-active controller for use in determining the input current to the MR damper. A semi-active controller is created based on a clipped-optimal control algorithm and controller weightings from Dyke *et al.* (1996).

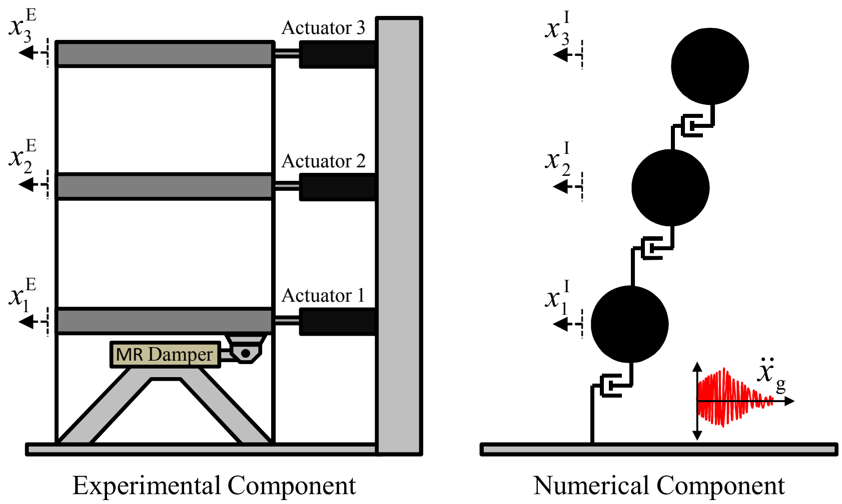

Figure 3.1. Three-story nonlinear structure

3.1. MIMO System Identification

In the likely case that the parameters of the specimen and servo-hydraulic system are unknown, nonparametric system identification can be used to obtain the servo-hydraulic system transfer function model (Kim *et al.*, 2005). As indicated previously, the model inverse has relatively few poles and zeros to fit. The simplicity of the inverse is the basis for the proposed system identification method for model-based multi-actuator control.

Step 1: Determine the experimental MIMO transfer function. The first step is to conduct system identification on coupled actuator system attached to specimen. One actuator should excite the specimen with a band-limited white-noise (BLWN) and the response be measured at all actuators. The process should be repeated for each actuator; the MIMO transfer function will thus be built one input at a time. During each test, the unexcited actuators should either be held at zero displacement or given a very low-amplitude BLWN to overcome static friction forces which can add damping to the system (Chang, 2011).

Step 2: MIMO transfer function inversion. At this step, the experimental MIMO transfer function should be inverted. The operation will be a matrix inversion at each frequency.

Step 3: Fitting the inverse. Next, each input-output pair of the inverse MIMO transfer function should be fit with a transfer function model. The transfer function models can then be combined to create an inverse MIMO transfer function model, which can be used as the feedforward controller. Insight from Eqn. 2.8 can aid in the model fitting.

Step 4: Creating the servo-hydraulic system transfer function model. The inverse of the inverse MIMO transfer function model will be equal to the servo-hydraulic system transfer function model. This model, in state space form, can be used for feedback control design. Note that when a MIMO transfer function model is converted into a state space model, it will not necessarily be a minimal realization. A minimal state space realization contains the minimal number of states necessary to represent the system dynamics. Such a realization is also necessarily both controllable and observable. Effort should be made to create a minimal realization; methods for creating minimal realizations are discussed in Chang (2011). Eqn. 2.9 demonstrates that a minimal realization is possible, whereby there are no duplicate or unnecessary states and all of the states are controllable through the actuators as well as observable using load cells and displacement transducers.

System identification is illustrated in Figs. 3.2 and 3.3 for the experimental component of Fig. 3.1.

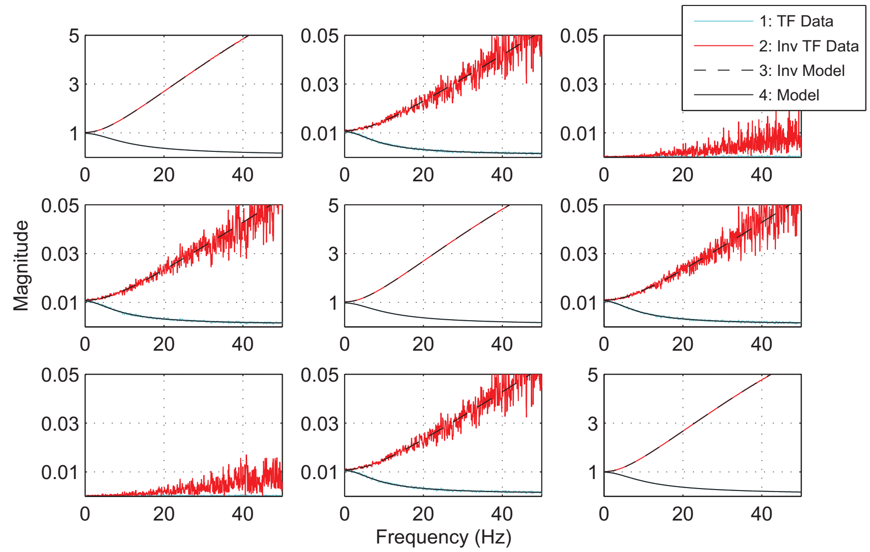

Figure 3.2. MIMO transfer function magnitude of the 3DOF experimental substructure

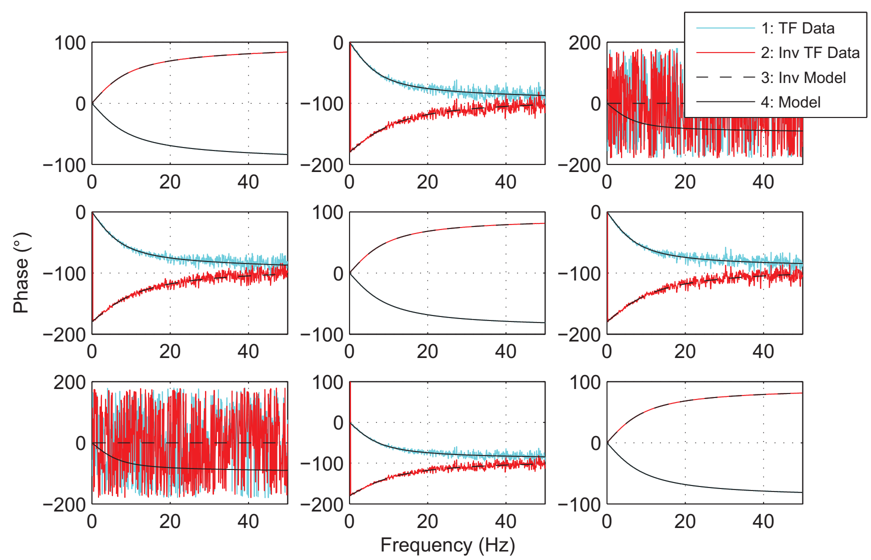

Figure 3.3. MIMO transfer function phase of the 3DOF experimental substructure

Each actuator is excited one at a time using a 0 to 50 Hz BLWN for a total of three data sets. During this excitation, the other actuators are held at zero displacement. Also, the MR damper is randomly switched from 0.0 to 2.0 Amps (0 to 2.25 V) to simulate semi-active conditions during RTHS. The fitted feedforward model contains three zeros in each of the diagonals, one zero in each of the immediate off-diagonals, and no dynamics for the extreme off-diagonals. The resulting servo-hydraulic system model contains six zeros and nine poles in the diagonals, four zeros and nine poles in each of the immediate off-diagonals, and two zeros and nine poles in the extreme off-diagonals.

3.2. RTHS Study

RTHS was used to evaluate the response of the three-story nonlinear structure employing semi-active control subjected to 0.5x the NS component of the 1940 El Centro earthquake. The simulation was run at 2000 Hz using the fourth-order Runge-Kutta scheme for numerical integration. Both the numerical and experimental components are simulated numerically using Matlab's Simulink environment with the effects of actuator dynamics included (as in Fig. 1.1). Model-based control is developed using the transfer function models in Figs. 3.2 and 3.3 obtained using system identification on the simulated experimental component. Simulated measurement noise is included in all feedback loops (e.g., restoring force of experimental component, measured displacement for model-based feedback control, and input for the semi-active controller). This noise is not included in the sampled measurements used for post-processing, equivalent to perfect filtering.

Six cases are considered to evaluate the structural response: (a) idealized simulation (i.e., no actuator dynamics, substructuring, or measurement noise), (b) RTHS with actuator dynamics and no compensation, (c) RTHS with actuator dynamics and model-based feedforward control which neglects actuator coupling, (d) RTHS with actuator dynamics and model-based feedforward control which considers actuator coupling, (e) RTHS with actuator dynamics and model-based feedforward-feedback control which neglects actuator coupling, and (f) RTHS with actuator dynamics and model-based feedforward-feedback control which considers actuator coupling.

The simulation case (a) is considered the exact solution from which a comparison of RTHS cases (b) through (f) will be made. For case (b), the RTHS immediately went unstable, illustrating the need for actuator control in the presence of actuator dynamics. As a representative case, (f) is presented alongside case (a) in Fig. 3.4 for displacement and absolute acceleration of the first story, as well as MR damper hysteresis loops. Excellent correlation between the two cases is observed.

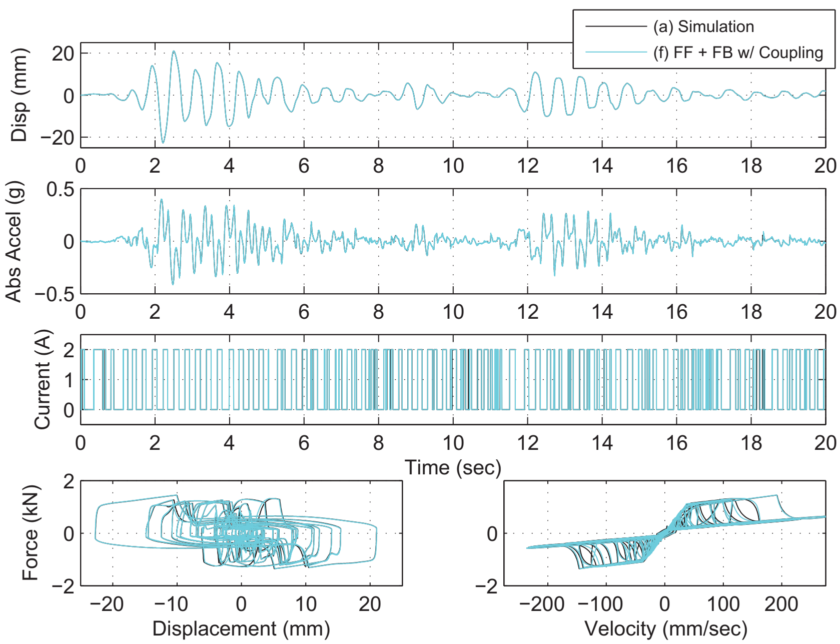

Figure 3.4. First story time histories and MR damper hysteresis

Graphically distinguishing cases (c) through (f) is difficult. Therefore, RMS error norm will be used as a quantitative measure of actuator controller performance. Comparisons are made for cases (c) through (f) in Table 3.1 for both tracking error (RMS error norm between desired and measured displacements) and response error (RMS error norm between displacements/accelerations of RTHS compared to the exact solution). Tracking error illustrates how well the actuator controller performs physically tracking the desired displacements. Response quantity errors illustrate how much the RTHS solution is diverging from the ideal simulation solution. With semi-active control, where future control efforts depend on past responses, solutions can diverge quickly due to small differences.

In this study, the effect of actuator coupling is investigated along with the benefits of feedback control. In cases when actuator coupling is neglected (i.e., ignoring off-diagonal terms of Eqn. 2.8 and 1.5 for feedforward and feedback controller designs, respectively), appreciable tracking error is found, leading to large response error. On the other hand, considering actuator coupling when designing multi-actuator control significantly improves the accuracy of the RTHS as measured by both tracking error and response error. As the amount of actuator coupling increases, for example due to a stiffer specimen, the benefits of considering the coupling for control design will also increase. In all cases, feedback control improves the accuracy of the RTHS compared to feedfoward control alone. Because the feedforward controller is based on a linear model of the servo-hydraulic system, the feedback controller will add robustness to changing specimen conditions, modeling errors, and nonlinearities.

Table 3.1. RMS Error of Tracking and Response for Actuator Control Strategies.

Actuator Control Strategy	Tracking Error (%)			Response Error (%)					
	e_1	e_2	e_3	x_1	x_2	x_3	$\ddot{x}_1$	$\ddot{x}_2$	$\ddot{x}_3$
(c) FF w/o Coupling	1.71	1.99	0.910	8.92	8.75	8.77	20.1	13.2	12.2
(d) FF w/ Coupling	0.133	0.009	0.009	1.50	1.36	1.36	7.79	4.61	3.14
(e) FF + FB w/o Coupling	0.470	0.547	0.248	2.76	2.70	2.68	8.85	5.59	4.31
(f) FF + FB w/ Coupling	0.045	0.003	0.003	1.34	1.26	1.25	7.09	4.14	2.76

4. CONCLUSIONS

This paper proposed a control approach for RTHS of multi-actuator systems. First, the source of actuator coupling for multi-actuator systems was illustrated by example. Subsequently, a framework for model-based multi-actuator control including both feedforward and feedback links was developed that directly addresses dynamics in the RTHS loop including CSI. A simple approach to identifying the servo-hydraulic transfer function model and its inverse for designing a model-based controller was also outlined. The model-based multiple-actuator controller performed very well during the simulated RTHS of a three-story nonlinear structure. Through this example, the benefit of considering actuator coupling in actuator control was demonstrated. Feedback control was shown to further improve the performance of the feedforward controller alone for the nonlinear structure.

ACKNOWLEDGEMENTS
The authors would like to acknowledge the support of the National Science Foundation award CMMI-1011534.

REFERENCES

Carrion, J.E. and Spencer Jr., B.F. (2007). "Model-based strategies for real-time hybrid testing." *Newmark Structural Engineering Laboratory Report Series*, University of Illinois at Urbana-Champaign, Urbana, IL, No. 6.

Chang, C.M. (2011). "Multi-axial active isolation for seismic protection of buildings." PhD Thesis, University of Illinois at Urbana-Champaign, Urbana, Illinois.

Dyke, S.J., Spencer Jr., B.F., Quast, P., and Sain, M.K. (1995). "Role of control-structure interaction in protective system design." *Journal of Engineering Mechanics,* **121:2**, 322-338.

Dyke, S.J., Spencer Jr., B.F., Sain, M.K., and Carlson, J. D. (1996). "Modeling and control of magnetorheological dampers for seismic response reduction." *Smart Materials and Structures*, **5:5**, 565-575.

Kim, S.B., Spencer Jr., B.F., Yun, C.B. (2005). "Frequency domain identification of multi-input, multi-output systems considering physical relationships between measured variables." *Journal of Engineering Mechanics*, **131:5**, 461-473.

Lewis, F.L. and Syrmos, V.L. (1995). *Optimal Control*. Second Edition. Wiley-Interscience, John Wiley & Sons, Inc., New York, pp. 377-393.

Phillips, B.M. and Spencer Jr., B.F. (2011). "Model-based feedforward-feedback tracking control for real-time hybrid simulation." *Newmark Structural Engineering Laboratory Report Series*, University of Illinois at Urbana-Champaign, Urbana, IL, No. 28.

Spencer Jr., B.F., Dyke, S.J., Sain, M.K., and Carlson, J.D. (1997). "Phenomenological model for magnetorheological dampers." *Journal of Engineering Mechanics*, **123:3**, 230-238.